

Article

Performance of Particulate and Structured Pt/TiO₂-Based Catalysts for the WGS Reaction under Realistic High- and Low-Temperature Shift Conditions

Andreas Kouroumlidis ¹, Georgios Bamos ^{1,*} , Paraskevi Panagiotopoulou ² and Dimitris I. Kondarides ¹¹ Department of Chemical Engineering, University of Patras, 6504 Patras, Greece² School of Chemical and Environmental Engineering, Technical University of Crete, 73100 Chania, Greece

* Correspondence: geoba@chemeng.upatras.gr; Tel.: +30-2610997223

Abstract: The water–gas shift (WGS) activity of Pt/TiO₂-based powdered and structured catalysts was investigated using realistic feed compositions that are relevant to the high-temperature shift (HTS) and low-temperature shift (LTS) reaction conditions. The promotion of the TiO₂ support with small amounts of alkali- or alkaline earth-metals resulted in the enhancement of the WGS activity of 0.5%Pt/TiO₂(X) catalysts (X = Na, Cs, Ca, Sr). The use of bimetallic (Pt–M)/TiO₂ catalysts (M = Ru, Cr, Fe, Cu) can also shift the CO conversion curve toward lower temperatures, but this is accompanied by the production of relatively large amounts of unwanted CH₄ at temperatures above ca. 300 °C. Among the powdered catalysts investigated, Pt/TiO₂(Ca) exhibited the best performance under both HTS and LTS conditions. Therefore, this material was selected for the preparation of structured catalysts in the form of pellets as well as ceramic and metallic catalyst monoliths. The 0.5%Pt/TiO₂(Ca) pellet catalyst exhibited comparable activity with that of a commercial WGS pellet catalyst, and its performance was further improved when the Pt loading was increased to 1.0 wt.%. Among the structured catalysts investigated, the best results were obtained for the sample coated on the metallic monolith, which exhibited excellent WGS performance in the 300–350 °C temperature range. In conclusion, proper selection of the catalyst structure and reaction parameters can shift the CO conversion curves toward sufficiently low temperatures, rendering the Pt/TiO₂(Ca) catalyst suitable for practical applications.

Keywords: water gas shift; platinum; TiO₂; promoter; structured catalysts; pellets; monoliths

Citation: Kouroumlidis, A.; Bamos, G.; Panagiotopoulou, P.; Kondarides, D.I. Performance of Particulate and Structured Pt/TiO₂-Based Catalysts for the WGS Reaction under Realistic High- and Low-Temperature Shift Conditions. *Catalysts* **2023**, *13*, 372. <https://doi.org/10.3390/catal13020372>

Academic Editor: Rufino Navarro Yerga

Received: 14 January 2023

Revised: 31 January 2023

Accepted: 6 February 2023

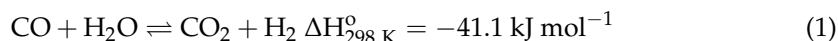
Published: 8 February 2023



Copyright: © 2023 by the authors. Licensee MDPI, Basel, Switzerland. This article is an open access article distributed under the terms and conditions of the Creative Commons Attribution (CC BY) license (<https://creativecommons.org/licenses/by/4.0/>).

1. Introduction

The water–gas shift (WGS) reaction (Equation (1)) is a well-established industrial process that is commonly used to reduce the CO concentration and increase the hydrogen content in the synthesis gas produced via reforming/partial oxidation of carbon-containing fuels [1–4].



The reaction is equilibrium-controlled and moderately exothermic and is therefore thermodynamically favored at low temperatures, and kinetically favored at high temperatures. As a result, the reaction is typically performed in industrial processes using two adiabatic reactors in sequence, with intermediate cooling. The first reactor operates at 350–450 °C using a Fe–Cr based oxide catalyst (high-temperature shift, HTS), and the second at 200–250 °C using Cu–Zn based catalysts (low-temperature shift, LTS) [1–4]. The inherent disadvantages of the classic commercial HTS catalysts (e.g., toxicity of hexavalent Cr and demanding reduction process to avoid sintering) and LTS catalysts (e.g., relatively low activity, pyrophoricity, thermal sintering, and leaching of active component) render them unsuitable for mobile and small-to-medium scale applications [2,3,5]. Therefore, efforts are currently focused on the development of alternative WGS catalysts that fulfill

the requirements for use in compact fuel processors. In this respect, metal oxide-supported noble metals have been extensively studied due to their superior kinetic performance and stability under frequent start-up/shut-down and varied duty cycle operations [1,4–6]. Among the noble metal catalysts investigated, platinum supported on partially reducible oxides such as CeO₂ and TiO₂ exhibit the highest WGS activity [1,7–9]. However, most of the above studies reported results with powder catalyst samples, which are not directly relevant to practical applications where the catalyst is in the form of pellets or monoliths. Pellets provide a high surface area of catalyst per unit reactor volume and are easy to handle and replace, whereas monolithic catalysts offer several advantages including lower pressure drop, good thermal shock resistance, robustness, and fast response to transient operation [10,11]. The competitive performance of structured noble metal-containing WGS catalysts has been investigated in several studies [6,10–17], but only a few of them have been performed under realistic reaction conditions. In our previous work, we investigated in detail the performance for the WGS reaction of noble metal catalysts (Pt, Rh, Ru, Pd) dispersed on reducible (TiO₂, CeO₂, La₂O₃, YSZ) and irreducible (Al₂O₃, MgO, SiO₂) metal oxide supports [7,8]. Among the metal–support combinations investigated, Pt/TiO₂ was found to exhibit the highest WGS activity, which could be further enhanced following the promotion of TiO₂ with small amounts of alkali (Li, Na, K, Cs) [18] or alkaline earth metals (Mg, Ca, Sr, Ba) [19]. This has been attributed to the promoter-induced creation of dual function Pt – □_s – Ti³⁺ sites at the metal–support interface, where □_s denotes an oxygen defect, which are required for the WGS reaction to proceed. The adsorption strength of these sites toward hydrogen was found to depend on the nature of the promoter and decreased with an increase in its content [18–20].

The objective of the present work was to investigate the performance of the previously developed Pt/TiO₂-based catalysts under realistic reaction conditions using feed compositions that are relevant to the HTS and LTS reactions. The effects of the dispersion of a second metal (Fe, Cu, Cr, Ru) on the support were also studied. The performance of the optimized catalysts in the form of pellets or wash-coating on ceramic and metallic monoliths was further investigated under realistic conditions and was compared with that of a commercial catalyst obtained from Johnson Matthey. To the best of our knowledge, this is one of the few reports to deal with the development of structured Pt/TiO₂-based catalysts and testing under HT- and LT-WGS conditions that are relevant to practical applications and can be regarded as an essential step toward the commercialization of these materials.

2. Results and Discussion

The powdered and structured catalysts synthesized are listed in Table 1. The composition of the Pt/TiO₂(X) catalysts (X = Na, Cs, Ca, Sr) was selected based on the results of our previous studies, which showed that the WGS activity of platinum dispersed on alkali- and alkaline earth metal-promoted TiO₂ exhibited a volcano-type dependence on the promoter content and was maximized for samples containing 0.06 wt.% Na, 0.34 wt.% Cs, 2.0 wt.% CaO, or 1.0 wt.% SrO [18,19]. Regarding the bimetallic (Pt–M)/TiO₂ catalysts (M = Ru, Fe, Cr, Cu), the second metal (M) was chosen based on the well-known activity of Fe/Cr and Cu for the HTS and LTS reactions, respectively, [1–4] and the high WGS activity of Ru supported on reducible metal oxides [7,8].

Table 1. Physicochemical characteristics of the synthesized catalysts.

Catalyst Notation	Nominal Composition (wt.%)	Specific Surface Area (SSA) ¹ (m ² /g)	Anatase Content ² (%)	Pt Dispersion ³ (%)	Pt Crystallite Size ³ (nm)
Pt/TiO ₂	0.5%Pt/TiO ₂	49	85	85	1.2
Pt/TiO ₂ (Na)	0.5%Pt/TiO ₂ (0.06%Na)	30	47	93	1.1
Pt/RiO ₂ (Cs)	0.5%Pt/TiO ₂ (0.34%Cs)	31	58	95	1.1
Pt/TiO ₂ (Ca)	0.5%Pt/TiO ₂ (2%CaO)	40	65	78	1.3
Pt/TiO ₂ (Sr)	0.5%Pt/TiO ₂ (1%SrO)	38	62	94	1.1
(Pt–Ru)/TiO ₂	(0.5%Pt–0.1%Ru)/TiO ₂	46	68	n.m. ⁴	n.m.

Table 1. Cont.

Catalyst Notation	Nominal Composition (wt.%)	Specific Surface Area (SSA) ¹ (m ² /g)	Anatase Content ² (%)	Pt Dispersion ³ (%)	Pt Crystallite Size ³ (nm)
(Pt-Fe)/TiO ₂	(0.5%Pt-0.5%Fe)/TiO ₂	49	67	n.m.	n.m.
(Pt-Cr)/TiO ₂	(0.5%Pt-0.5%Cr)/TiO ₂	50	62	n.m.	n.m.
(Pt-Cu)/TiO ₂	(0.5%Pt-0.5%Cu)/TiO ₂	45	66	n.m.	n.m.
TiO ₂ -P	TiO ₂ pellets	42	n.m.	n.m.	n.m.
0.5Pt/TiO ₂ (Ca)-P	0.5%Pt/TiO ₂ (2%CaO) pellets	37	n.m.	90	1.1
1.0Pt/TiO ₂ (Ca)-P	1.0%Pt/TiO ₂ (2%CaO) pellets	38	n.m.	92	1.1
Pt/TiO ₂ (Ca)-MM	0.5%Pt/TiO ₂ (2%CaO) coated on metallic monolith				
Pt/TiO ₂ (Ca)-CM	0.5%Pt/TiO ₂ (2%CaO) coated on ceramic monolith				

¹ Estimated with the BET method; ² Anatase content of TiO₂ calculated from the XRD patterns; ³ Estimated from the H₂ chemisorption measurements; ⁴ Not measured.

2.1. Physicochemical Characteristics of the Synthesized Catalysts

The X-ray diffraction (XRD) patterns obtained for the representative powdered catalysts are shown in Figure 1. It was observed that, in all cases, the diffractograms consisted of peaks attributable to the anatase (JCPDS Card No. 4-477) and rutile (JCPDS Card No. 21-1276) phases of TiO₂. Qualitatively similar results were obtained for all of the catalyst samples investigated (not shown for brevity). The specific surface area (SSA) and anatase content of TiO₂ (x_A) were considerably lower for the samples promoted with Na or Cs compared to the unpromoted Pt/TiO₂ (Table 1). This can be attributed to the synthesis method employed, which involved the heat treatment of the corresponding supports at 600 °C. This treatment is known to result in the partial transformation of the anatase phase of TiO₂ to rutile and is accompanied by particle growth and a decrease in the SSA [19]. In contrast, the SSA and anatase content were partially retained for the alkaline earth (Ca, Sr)-promoted catalysts (Table 1). This is in agreement with the results of our previous studies, which showed that the incorporation of foreign cations in the crystal matrix of TiO₂ resulted in an increase in the anatase-to-rutile phase transition temperature and in the stabilization of the specific surface area of the host material [19,21]. Regarding the bimetallic (Pt-M)/TiO₂ (M = Ru, Fe, Cr, Cu) catalysts, it was observed that their SSA and anatase content were not significantly different compared to the unpromoted Pt/TiO₂ sample (Table 1).

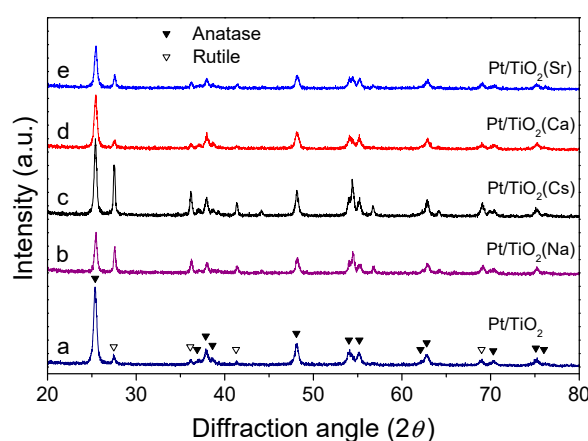


Figure 1. X-ray diffraction patterns of the indicated catalysts. (a) Pt/TiO₂; (b) Pt/TiO₂(Na); (c) Pt/TiO₂(Cs); (d) Pt/TiO₂(Ca); (e) Pt/TiO₂(Sr).

The average crystallite size of the TiO₂ particles, estimated using the Scherrer equation, did not vary appreciably from one catalyst to another, taking values in the ranges of 20–26 nm for anatase and 25–35 nm for rutile for all of the samples investigated. Therefore, the observed differences in the performance of these samples should not be attributed to this parameter, which is known to affect the WGS activity of TiO₂-supported Pt catalysts [7].

The Pt dispersion and average crystallite size were estimated for the monometallic catalysts from the H₂ chemisorption measurements and the results obtained are listed in Table 1. It should be noted that this method could not be applied for the bimetallic (Pt–M) samples because hydrogen interacts with both metals. It was observed that Pt was very well-dispersed on all supports studied, forming crystallites with an average size in the range 1.1–1.3 nm.

Representative TEM images obtained for the Pt/TiO₂ and Pt/TiO₂(Ca) catalysts are shown in Figure 2. It was observed that platinum was very well-dispersed on the surface of both the TiO₂ (Figure 2a) and TiO₂(Ca) (Figure 2b) supports. The size of the Pt crystallites was in the range of 1–2 nm, in very good agreement with the results of the H₂-chemisorption measurements (Table 1). The SEM images with EDS mapping of the above two catalysts are shown in the Supplementary Materials (Figures S1 and S3). It was observed that Pt was homogeneously distributed on the surface of both catalysts (Figures S1 and S3), and the same was true for the Ca present in the TiO₂(Ca) support (Figure S2).

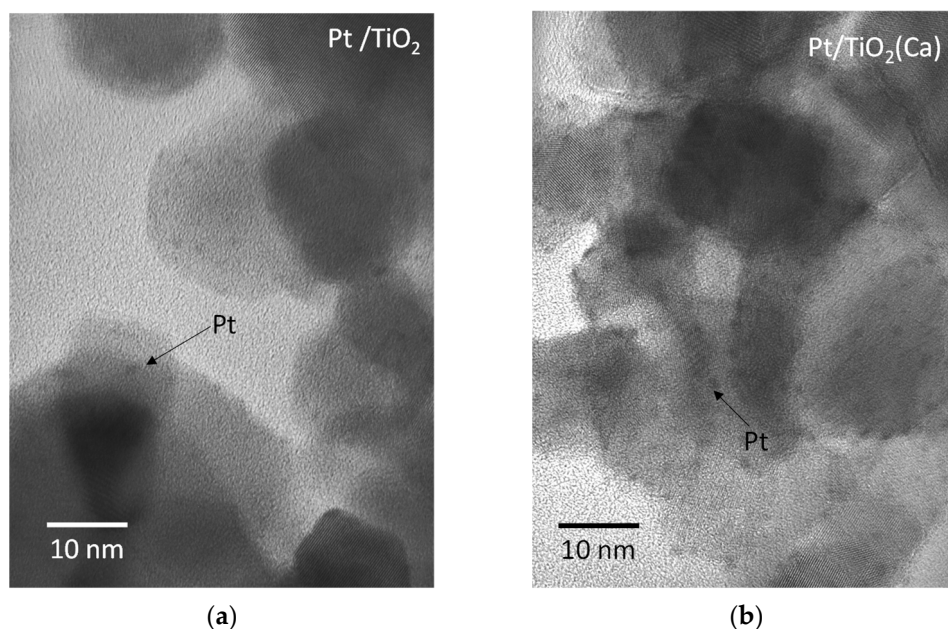


Figure 2. The TEM images of the (a) Pt/TiO₂ and (b) Pt/TiO₂(Ca) powdered catalysts.

2.2. Performance of Particulate Catalysts

2.2.1. Alkali- and Alkaline Earth Metal-Promoted Catalysts

The WGS activity of the synthesized alkali- and alkaline earth-promoted Pt/TiO₂ catalysts was investigated using two different feed compositions, which are representative of the high temperature shift (HTS) and the low temperature shift (LTS) reaction conditions. Figure 3a shows the CO conversion curves obtained under HTS conditions. It was observed that the unpromoted Pt/TiO₂ catalyst became active at temperatures around 250 °C. Conversion of CO (X_{CO}) progressively increased with the increase in the temperature and reached equilibrium at ca. 450 °C. Promotion of the TiO₂ support with small amounts of alkali metals resulted in a significant enhancement in the WGS activity, which was evidenced by the shift of the CO conversion curves obtained for the Pt/TiO₂(Na) and Pt/TiO₂(Cs) catalysts toward lower temperatures by ca. 40 °C and 50 °C, respectively, compared to the unpromoted sample. The performance of the two alkaline earth metal-promoted catalysts was even better than that of the alkali-promoted samples. Optimal results were obtained for Pt/TiO₂(Ca), which achieved an equilibrium CO conversion at ca. 390 °C (Figure 3a).

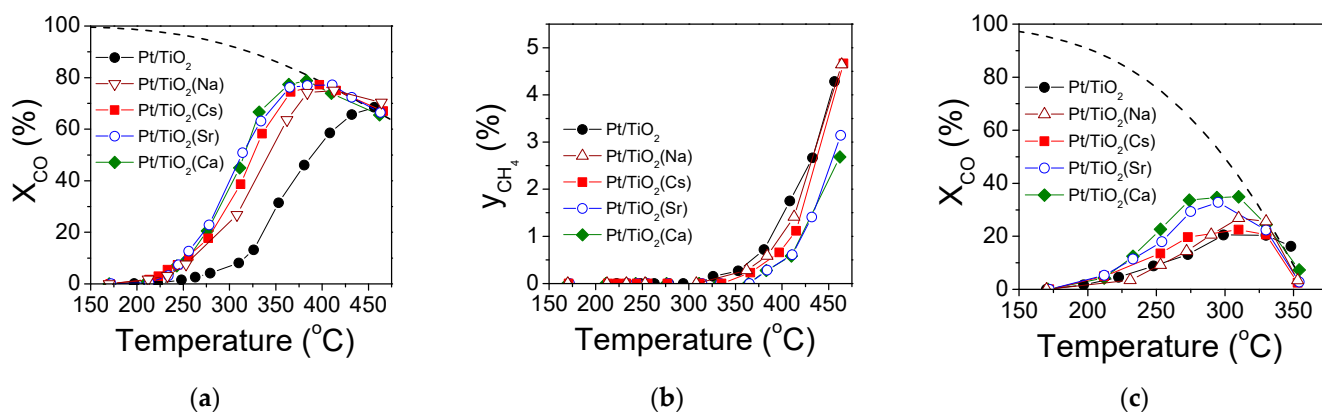
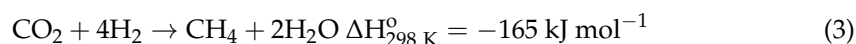
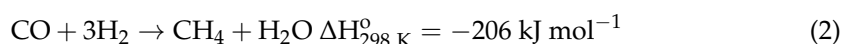


Figure 3. Performance of the alkali- and alkaline earth metal-promoted catalysts: Effect of reaction temperature on (a) the conversion of CO and (b) the yield of CH₄ under HTS conditions (feed composition: 9.7%CO, 38.7%H₂O, 44.8%H₂, 6.8%CO₂). (c) Effect of reaction temperature on the conversion of CO under LTS conditions (feed composition: 1.6%CO, 29.9%H₂O, 52.2%H₂, 16.3%CO₂). Mass of the catalyst: 750 mg; total flow rate: 220 cm³ min⁻¹. The equilibrium CO conversion curves are shown with dashed lines.

Under the HTS conditions employed in Figure 3a, all samples catalyzed the CO/CO₂ methanation reactions at elevated temperatures:



These reactions are unwanted because they reduce the yield of H₂ and may result in large exotherms. As shown in Figure 3b, methane formation started at ca. 320 °C and the yield of methane (y_{CH_4}) increased considerably with the increase in the reaction temperature. Interestingly, the best performing HTS catalysts, namely, Pt/TiO₂(Ca) and Pt/TiO₂(Sr), produced lower amounts of methane compared to the unmodified Pt/TiO₂ and the alkali-promoted samples. It should be noted that the occurrence of the CO methanation reaction in parallel to the WGS reaction can explain the observation that X_{CO} slightly exceeded the equilibrium CO conversion at high temperatures under these conditions (Figure 3a).

Results of the catalytic performance tests obtained under LTS conditions are shown in Figure 3c. It was observed that catalyst ranking follows the same trend with that of the HTS experiments, with Pt/TiO₂(Ca) exhibiting the highest activity. It should be noted that under the LTS conditions, only negligible amounts of CH₄ were detected at the reactor effluent in the temperature range investigated.

In our previous studies [18–20], the enhanced WGS activity of the alkali/alkaline earth-promoted Pt/TiO₂ catalysts was attributed to the creation of Pt – □_s – Ti³⁺ active sites located at the metal–support interface. The population of this type of site is expected to increase under conditions that favor the decoration of the metal crystallites by TiO_x suboxides [22], in accordance with the SMSI effect [8,18,20,23–26]. It should be noted, however, that the SMSI effect is not expected to be significant under the conditions employed here. This is because the migration of suboxide species on the surface of dispersed metal crystallites is known to become important following reduction at temperatures typically higher than 500 °C and is not operable in the presence of water [23,24]. The promotion of TiO₂ by alkali/alkaline earth metals induces the same effect as SMSI as it also leads to the creation of □_s – Ti³⁺ defects. Moreover, this is undertaken in a controlled manner, depending on the dopant content, and is permanent. Therefore, it can be viewed as a “permanent” SMSI effect [18,20].

2.2.2. Bimetallic Catalysts

An attempt was made to enhance the WGS activity of the 0.5%Pt/TiO₂ catalyst by dispersing a second metal (M = Ru, Fe, Cr, Cu) on the support, in addition to Pt. Results obtained for the HTS reaction over the (0.5%Pt–0.5%M)/TiO₂ catalysts are shown in Figure 4a. It was observed that the addition of a component of commercial LTS catalysts [3], resulted in a significant shift in the CO conversion curve toward higher temperatures compared with the monometallic Pt/TiO₂ sample. On the other hand, the addition of Fe or Cr, which are components of commercial HTS catalysts [3], has a favorable effect as the X_{CO} curves shift toward lower temperatures by ca. 10–20 °C. A similar and more pronounced beneficial effect was observed following the addition of Ru. However, the (Pt–Ru)/TiO₂ catalyst promotes the unwanted CO/CO₂ methanation reactions at elevated temperatures (Figure 4b), rendering it unsuitable for practical applications. This observation is in agreement with the results of our previous study, which showed that the CO/CO₂ methanation activity of Ru was higher than that of Pt, and was not significantly affected by the presence of water in the feed [27]. Regarding the activity of (Pt–M)/TiO₂ catalysts under LTS conditions, all samples were less active compared to the monometallic Pt/TiO₂ (Figure 4c).

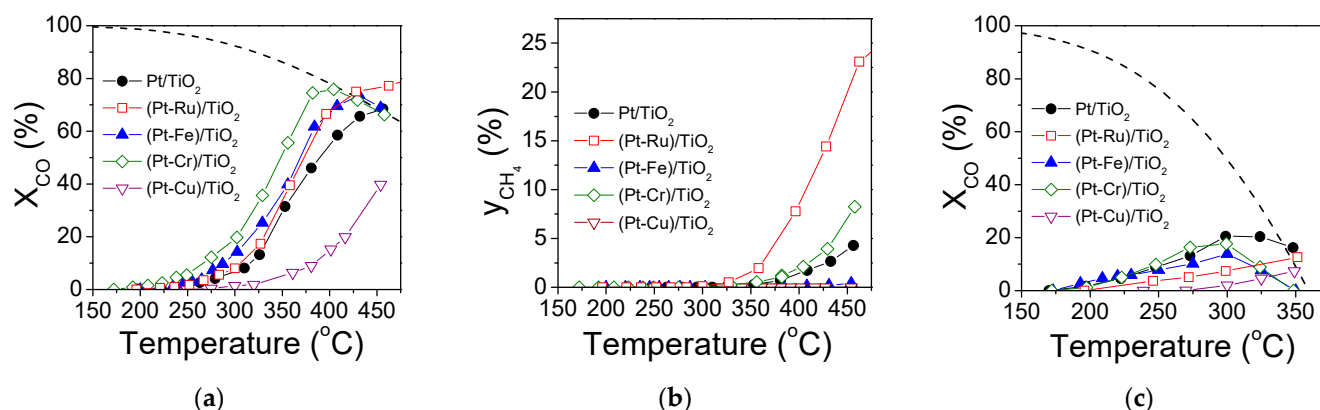


Figure 4. Performance of the bimetallic catalysts: Effect of reaction temperature on (a) the conversion of CO and (b) the yield of CH₄ under HTS conditions. (c) Effect of reaction temperature on the conversion of CO under LTS conditions. Experimental conditions are the same as in Figure 3.

Increasing the Fe or Cr loading of the bimetallic catalysts resulted in decreased performances under both the HTS and LTS conditions. Typical results obtained over the (0.5%Pt–M)/TiO₂ catalysts are shown in the Supplementary Materials (Figure S4). It was observed that increasing the Fe or Cr content from 0.5% to 5.0% resulted in a shift in the CO conversion curves toward higher temperatures, which was more pronounced for (Pt–Cr)/TiO₂. The yield of methane did not vary appreciably with increasing the Fe or Cr content from 0.5 to 5.0 wt.%. Furthermore, it was found that the performance of bimetallic Pt–M catalysts dispersed on the optimal TiO₂(Ca) support does not result in materials with improved WGS activity, compared to the monometallic Pt/TiO₂(Ca) sample (results not shown for brevity).

2.3. Performance of Structured Catalysts

Results presented in Figures 3 and 4 show that, among the alkali/alkaline earth metal-promoted Pt/TiO₂(X) catalysts and the bimetallic (Pt–M)/TiO₂ catalysts investigated, 0.5%Pt/TiO₂(Ca) exhibited the best performance under both the HTS and LTS reaction conditions. Therefore, this material was selected to prepare structured catalysts in the form of pellets or coatings on ceramic and metallic monoliths to investigate its performance for the WGS reaction under conditions that are more relevant to practical applications. The performance of the above structured samples was compared with that of a commercial catalyst in pellet form obtained from Johnson Matthey (JM) (Product name: W21, 10876, UK).

Results obtained over the structured catalysts with the use of the feed composition corresponding to the HTS conditions are presented in Figure 5a, where the conversion of CO is plotted as a function of the reaction temperature (measured at the exit of the catalyst bed). Regarding the 0.5%Pt/TiO₂(Ca)-P catalyst (i.e., in pellet form), it was observed that X_{CO} became measurable at temperatures around 200 °C and reached equilibrium at ca. 400 °C. Comparison with the corresponding results obtained over the powdered Pt/TiO₂(Ca) sample (Figure 3a) showed that the present CO conversion curve shifted toward lower temperatures (by ca. 50 °C). This was due to the larger amount of catalyst loaded in the reactor (1.8 g vs. 0.75 g) under the same experimental conditions. The performance of the Pt/TiO₂(Ca)-P catalyst was considerably improved with an increase in the Pt loading from 0.5% to 1.0% (Figure 5a). This is in agreement with the results of our previous studies that showed that the CO conversion curve over TiO₂-supported noble metal catalysts shifted monotonically toward lower temperatures with an increase in the metal loading from 0.1 to 5.0 wt.% [7,8]. It should be noted, however, that the specific activity (TOF) did not vary appreciably with metal loading, indicating that the WGS is a structure insensitive reaction [7,8]. It is of interest to note that the 1.0%Pt/TiO₂(Ca) pellet catalyst achieved equilibrium CO conversion at a temperature around 330 °C and was more active than the commercial JM catalyst across the whole temperature range investigated (Figure 5a).

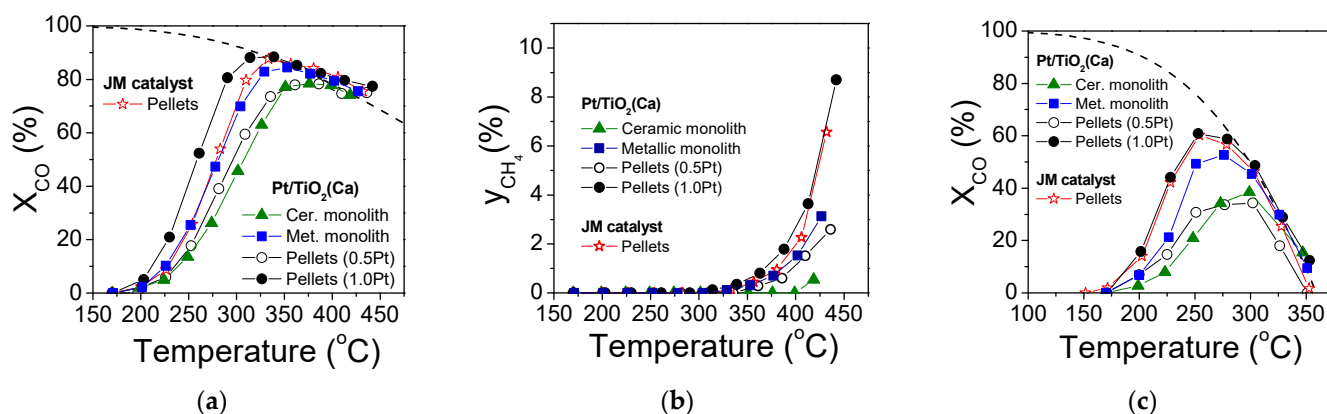


Figure 5. Performance of the structured Pt/TiO₂(Ca) catalysts in the form of pellets or coatings in the channels of ceramic and metallic monoliths in comparison with that of a commercial catalyst (Johnson Matthey, JM): Effect of reaction temperature on (a) the conversion of CO and (b) the yield of CH₄ under HTS conditions. (c) Effect of the reaction temperature on the conversion of CO under LTS conditions. Mass of the synthesized and JM catalyst pellets and the monolith coatings: 1.8 g. Other experimental conditions were the same as in Figure 3.

The CO conversion curve obtained for the ceramic monolith coated with 1.8 g of Pt/TiO₂(Ca) shifted toward slightly higher temperatures (ca. 10 °C) compared to the catalyst in the form of pellets (Figure 5a). On the other hand, the metallic monolith catalyst exhibited improved performance compared to the previous two samples, as the CO conversion reached equilibrium at ca. 350 °C. It is of interest to note that the performance of the latter sample was comparable to that of the commercial JM pellet catalyst. Under the experimental conditions in Figure 5a, all of the structured catalysts investigated produced methane at temperatures above ca. 320 °C (Figure 5b). The yield of methane followed the same trend as that of the WGS activity (i.e., it was lowest for Pt/TiO₂(Ca)-CM and highest for the 1.0Pt/TiO₂(Ca)-P and JM samples in the whole temperature range investigated) (Figure 5b).

The performance of the structured catalysts under the LTS conditions is shown in Figure 5c. It was observed that the best performing sample was 1.0%Pt/TiO₂(Ca)-P, which exhibited a similar performance with the commercial JM catalyst. Regarding the structured catalysts of the same Pt content (0.5 wt.%), the most active one was Pt/TiO₂(Ca)-MM. It

should be noted that the blank experiments performed over the bare ceramic and metallic monoliths did not show measurable CO conversion under the HTS and LTS conditions employed here.

The effects of the total flow rate (space velocity) on the WGS performance of the best-performing Pt/TiO₂(Ca)-MM catalyst are shown in Figure 6. Results of similar experiments performed over the cordierite monolithic catalyst are presented in the Supplementary Materials (Figure S5). As expected, an increase in the flow rate from 220 to 400 cm³ min⁻¹ resulted in a shift in the CO conversion curves toward higher temperatures under both the HTS and LTS conditions. On the other hand, the X_{CO} curves shifted toward lower temperatures upon decreasing the total flow rate to 100 cm³ min⁻¹. It is of interest to note that under these conditions and the use of the HTS feed, the Pt/TiO₂(Ca)-MM catalyst achieved equilibrium CO conversion at around 320 °C (Figure 6a), where the production of CH₄ is negligible (Figure 6b). The catalyst also performed well under LTS conditions, where equilibrium CO conversion was achieved at ca. 270 °C (Figure 6c).

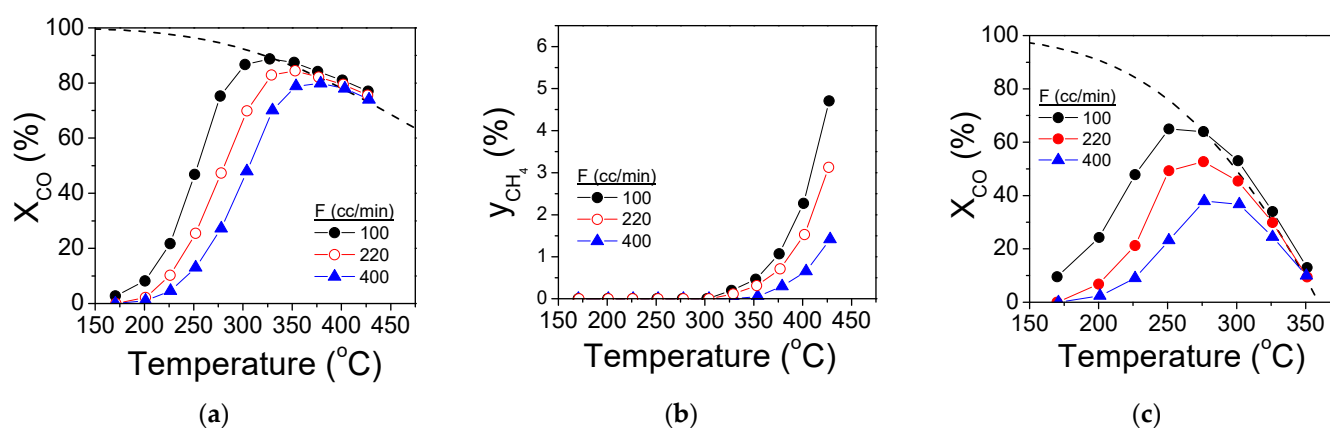


Figure 6. Effects of the total flow rate (F) on the performance of the Pt/TiO₂(Ca) catalyst coated on the channels of the metallic monolith: (a) Conversion of CO and (b) yield of CH₄ under HTS conditions. (c) Conversion of CO under LTS conditions. Other experimental conditions are the same as in Figure 5.

It should be noted that the temperature profile along the Pt/TiO₂(Ca)-MM catalyst was practically uniform under both the HTS and the LTS conditions employed here (see Supplementary Materials, Figure S6). In contrast, the temperature along the ceramic monolithic catalyst was found to increase toward the exit of the reactor (Figure S7). This was more pronounced under HTS conditions, elevated temperatures, and higher flow rates, where the CO conversion was also higher. This can be explained considering that metallic monoliths present high thermal conductivities and improved heat transfer characteristics compared to, for example, ceramic monoliths [15,28,29]. This advantage, combined with the easy fabrication and superior mechanical shock resistance of metallic monoliths, makes them suitable for practical applications.

The results presented in Figure 6a show that the Pt/TiO₂(Ca)-MM catalyst has the potential to be used in a single-step, medium temperature shift reactor operating in the 300–350 °C range to reduce the CO content in the reformed gas to ca. 1%, which can be tolerated by preferential oxidation (PROX) catalysts [1]. Replacing the two HTS and LTS reactors by a single medium-temperature reactor is highly desirable, especially for small-scale and mobile applications where volume/weight and ruggedness become more important [30,31]. The WGS performance of this catalyst may be further improved by optimizing the catalyst loading, washcoat thickness, and cell density of the monolithic substrate as well as by using novel multi-shelled and core-shell nano/microstructured catalyst formulations [32,33], the study of which was beyond the scope of the present work and may be the subject of our future investigation.

3. Materials and Methods

3.1. Catalyst Preparation

3.1.1. Powdered Catalysts

Titanium dioxide supports promoted with small amounts of alkali or alkaline earth metals, denoted as $\text{TiO}_2(\text{X})$ ($\text{X} = \text{Na}, \text{Cs}, \text{Ca}, \text{Sr}$), were prepared following the procedures described in detail elsewhere [18–20]. In a typical synthesis, a pre-weighed amount of commercial TiO_2 powder (Degussa P25) is added under continuous stirring in an aqueous solution containing the appropriate amount of the corresponding promoter salt, namely, NaNO_3 , CsNO_3 , $\text{Sr}(\text{NO}_3)_2$, or CaO (Alfa Aesar), the latter diluted in HNO_3 at $\text{pH} = 1$. The resulting dispersion was heated at $70\text{ }^\circ\text{C}$ and maintained at that temperature until nearly all the water had evaporated. The solid residue was dried overnight at $110\text{ }^\circ\text{C}$ and then calcined in stagnant air at $600\text{ }^\circ\text{C}$ for 5 h. The nominal contents (wt.%) of the promoters in the samples thus prepared were 0.06% for Na, 0.34% for Cs, 2.0% for CaO, and 1.0% for SrO (Table 1) and were selected based on their optimal concentrations derived in our previous studies [18–20].

Platinum catalysts dispersed on the pristine TiO_2 and the promoted $\text{TiO}_2(\text{X})$ supports were prepared via the wet impregnation method [7]. Briefly, a pre-weighed amount of the respective support was added under continuous stirring into an aqueous solution of $(\text{NH}_3)_2\text{Pt}(\text{NO}_2)_2$ (Alfa Aesar) followed by heating at $70\text{ }^\circ\text{C}$ to evaporate water, drying at $110\text{ }^\circ\text{C}$ overnight, and subsequent reduction under flowing H_2 at $300\text{ }^\circ\text{C}$ for 2 h. The nominal Pt loading of the catalysts thus prepared was 0.5 wt.%.

The bimetallic (Pt–M)/ TiO_2 catalysts ($\text{M} = \text{Fe}, \text{Cu}, \text{Cr}, \text{Ru}$) were synthesized by employing a two-step procedure. In the first step, the metal M (0.5 or 5.0 wt.%) was first deposited on the support following the impregnation of TiO_2 (P25) in an aqueous solution of the corresponding metal precursor salt, namely, $(\text{Fe}(\text{NO}_3)_3 \cdot 9\text{H}_2\text{O})$, $(\text{Cu}(\text{NO}_3)_2 \cdot 3\text{H}_2\text{O})$, $(\text{Cr}(\text{NO}_3)_3 \cdot 9\text{H}_2\text{O})$, or $(\text{Ru}(\text{NO})(\text{NO}_3)_3)$ (Alfa Aesar). This was followed by the evaporation of water at $70\text{ }^\circ\text{C}$, drying overnight at $110\text{ }^\circ\text{C}$, and subsequent calcination in stagnant air at $300\text{ }^\circ\text{C}$ for 3 h. Platinum (0.5 wt.%) was then added onto the resulting materials following the procedure described above.

3.1.2. Structured Catalysts

The best performing Pt/ $\text{TiO}_2(\text{Ca})$ catalyst was prepared in the form of pellets as well as in the form of coating on ceramic and metallic monoliths (Figure 7). Two pellet catalyst samples with different Pt loadings (0.5 and 1.0 wt.%) were synthesized as follows: An appropriate amount of CaO was diluted in an aqueous solution of HNO_3 ($\text{pH} = 1$) in a BUCHI beaker followed by the addition of TiO_2 pellets (Aerolyst 7711, 1/16"). The beaker was adjusted in a Rotavapor to remove water under vacuum at $40\text{ }^\circ\text{C}$. The pellets were then dried at $110\text{ }^\circ\text{C}$ overnight and subsequently calcined at $600\text{ }^\circ\text{C}$ for 5 h in stagnant air. The CaO-promoted TiO_2 pellets thus obtained were added in an aqueous $(\text{NH}_3)_2\text{Pt}(\text{NO}_2)_2$ solution contained in a BUCHI beaker adjusted to a Rotavapor. After the removal of water under vacuum at $40\text{ }^\circ\text{C}$, the pellets were dried overnight at $110\text{ }^\circ\text{C}$ and finally reduced under flowing H_2 at $300\text{ }^\circ\text{C}$ for 2 h.

The commercial catalyst used as the reference was supplied by Johnson Matthey and was in the form of 1/16" pellets (Product name: 205 W21, 10876, UK). No detailed information is available regarding the composition of this catalyst except that it contains a mixture of Al_2O_3 ($\geq 90\%$) and CeZrO_4 ($\leq 10\%$).

The ceramic monolithic catalyst was prepared by coating the Pt/ $\text{TiO}_2(\text{Ca})$ powder (see Section 3.1.1) in the channels of a cordierite monolith (400 cell per square inch, cpsi) of a cylindrical shape with a diameter of 2.4 cm and length of 3.6 cm. A hole was drilled at the center of the monolith (Figure 7b) to place a 1/16" quartz tube with a K-type thermocouple running throughout it to allow the temperature profile along the monolith to be monitored during the catalytic performance tests. The catalyst sample was first pulverized in a mortar and the resulting powder ($d < 63\text{ }\mu\text{m}$) was suspended under continuous stirring in triple-distilled water at a concentration of 0.33 g/mL. The monolith was then immersed in the

catalyst suspension, blown with compressed air to remove the excess slurry left in the channels, dried at 110 °C overnight, and subsequently calcined at 300 °C for 3 h in stagnant air. The amount of catalyst loaded was determined by weighing the monolith before and after the catalyst deposition. This procedure (immersion, drying, calcination, weighing) was repeated until the desired amount of catalyst (1.8 g) was deposited in the channels of the monolith.

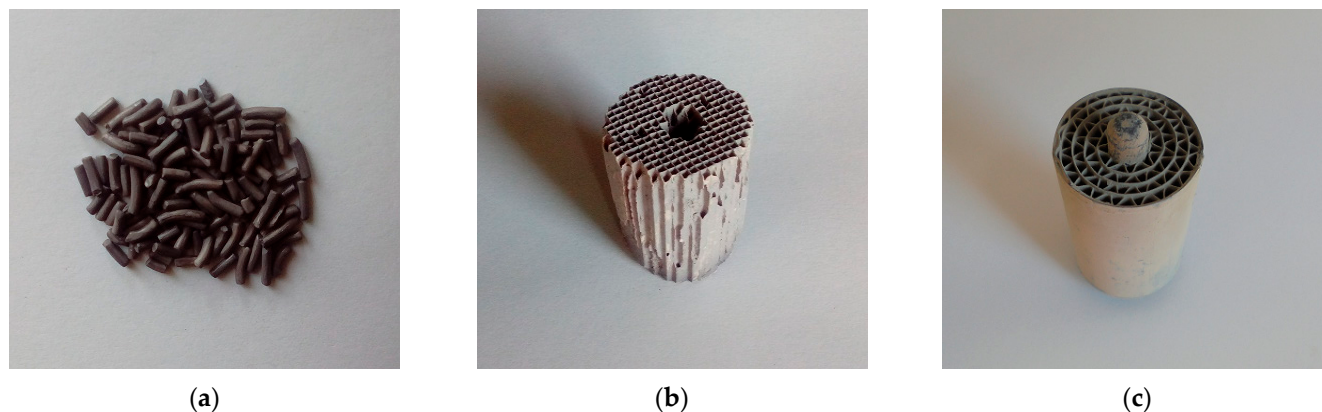


Figure 7. Photographs of the structured catalysts: (a) 1/16" pellets; (b) ceramic monolith; (c) metallic monolith.

A metallic monolith (custom made by rolling a corrugated Fe-Cr-Al alloy film, 300 cpsi) with the same dimensions as the ceramic monolith (diameter: 2.4 cm; length: 3.6 cm) was coated with the Pt/TiO₂(Ca) catalyst using the same technique. The total amount of catalyst deposited was 1.8 g.

3.2. Physicochemical Characterization

The specific surface areas (SSAs) of the synthesized catalysts were determined by employing the N₂ physisorption method at the temperature of liquid nitrogen (−196 °C) (BET method) on a Micromeritics (Gemini III 2375) instrument. Powder X-ray diffraction patterns were obtained in the 2θ range between 20° and 80° (scan rate 0.01° s^{−1}) on a Bruker D8 Advance (Cu Kα) apparatus operated at 40 kV and 40 mA, and were analyzed using JCPDS data files. The anatase content of TiO₂ in the catalyst samples was estimated from the following equation [7].

$$x_A = [1 + 1.26(I_R / I_A)]^{-1} \quad (4)$$

where I_A and I_R are the integral intensities of the anatase (101) and rutile (110) reflections, respectively.

Hydrogen chemisorption measurements were performed at 25 °C on a modified Fisons Instruments (Sorptomatic 1900) apparatus and the results were used to estimate the Pt dispersion and average crystallite size. Details of the experimental procedure and methods employed can be found elsewhere [7].

Transmission electron microscopy (TEM) images were recorded on a JEOL JEM-2100 apparatus (JEOL, Tokyo, Japan) operated at 200 kV (point resolution 0.23 nm) by means of an Erlangshen CCD Camera (Gatan Model 782 ES500W, Pleasanton, CA 94588, United States). SEM images were obtained using a JEOL 6300 scanning electron microscope (Akishima, Tokyo, Japan) equipped with an energy dispersive spectrometer (EDS, ISIS Link 300, Oxford Instruments, UK).

3.3. Catalytic Performance Tests

The experimental setup employed for the investigation of the WGS activity of the synthesized catalysts consisted of a flow system, a down-flow reactor, and an analysis

system. The flow system was equipped with mass flow controllers to adjust the flow of gases (He, CO, CO₂, H₂) and an HPLC pump (Marathon II) for feeding H₂O. Water was pumped into an evaporator operating at 170 °C and then mixed with the gas coming from the mass flow controllers. The resulting mixture was fed into the reactor through insulated stainless-steel tubing heated at 170 °C. The reactor consisted of a quartz tube (6 mm OD) with an expansion in its upper part (12 mm in the case of powdered samples; 20 mm in the case of pellets and 32 mm in the case of monoliths) where the catalyst sample was placed. The monoliths were wrapped with quartz wool to avoid by-pass flow. The oven temperature was controlled using a K-type thermocouple located between the oven walls and the reactor. The temperature profile at the catalyst bed was measured with a mobile K-type thermocouple placed in a thin quartz tube (1/16") running through the reactor. The reactor effluent passed through a condenser to trap unreacted H₂O and was then introduced to the analysis system, which consisted of a gas chromatograph (Shimadzu GC 14B) operating with He as the carrier gas, equipped with two columns (Porapak Q and Carbosieve) and two detectors (TCD and FID). Porapak Q was used for the separation of CH₄, C₂H₄, C₂H₆, C₃H₆, and C₃H₈ whereas Carbosieve was used for the separation of CO, CO₂, and CH₄.

Catalytic performance tests were performed at near atmospheric pressure in the temperature range of 170–450 °C using two different feed compositions: one corresponding to the HTS conditions (9.7%CO, 38.7%H₂O, 44.8%H₂, 6.8%CO₂) and one corresponding to the LTS conditions (1.6%CO, 29.9%H₂O, 52.2%H₂, 16.3%CO₂), which are relevant to practical applications [1]. Unless otherwise indicated, the total flow rate was 220 cm³ min⁻¹. The amount of catalyst used for the powdered samples (0.18 < *d* < 0.25 mm) was 750 mg, which corresponds to a space velocity of ca. 10,000 h⁻¹. For the structured samples, the amount of catalyst in the form of pellets or coating on the monoliths was 1.8 g (W/F= 0.5 g s cm⁻³). In a typical experiment, the catalyst was heated under He flow at 300 °C where the sample was in situ reduced under H₂ flow (60 cm³ min⁻¹) for 1 h. The temperature was then increased to 450 °C under He flow and the feed was switched to the reaction mixture. Measurements were recorded after conditioning of the catalyst for 1 h-on-stream. The reaction temperature was then stepwise decreased under the flowing reaction mixture and similar measurements were obtained. The CO conversion (*X*_{CO}) was calculated by employing the following equation:

$$X_{\text{CO}} = \frac{[\text{CO}]^{\text{in}} - [\text{CO}]^{\text{out}}}{[\text{CO}]^{\text{in}}} \times 100 \quad (5)$$

where [CO]ⁱⁿ and [CO]^{out} are the inlet and outlet concentrations of CO, respectively. The yield of methane (*y*_{CH₄}), which was formed at elevated temperatures via the methanation of CO (Equation (2)) and/or CO₂ (Equation (3)), was estimated using the equation:

$$y_{\text{CH}_4} = \frac{[\text{CH}_4]^{\text{out}}}{[\text{CO}]^{\text{in}} + [\text{CO}_2]^{\text{in}}} \times 100 \quad (6)$$

where [CH₄]^{out} is the outlet concentration of CH₄, and [CO]ⁱⁿ and [CO₂]ⁱⁿ are the inlet concentrations of CO and CO₂, respectively. All values reported are the averages of at least three measurements and correspond to the temperature measured at the outlet of the catalyst bed.

4. Conclusions

The WGS performance of 0.5%Pt/TiO₂(X) (X = Na, Cs, Ca, Sr) and (0.5%Pt-M)/TiO₂ (M = Fe, Cu, Cr, Ru) catalysts in powder form was investigated under realistic reaction conditions. The best results were obtained for the 0.5%Pt/TiO₂(Ca) catalyst, which exhibited high activity and selectivity toward H₂ under both HTS and LTS reaction conditions. The catalytic performance of the optimized catalyst in pellet form was comparable to

that of a commercial WGS pellet catalyst provided by JM and was further enhanced by increasing the Pt content from 0.5 to 1.0 wt.%. The results obtained using a ceramic and a metallic monolithic catalyst coated with 0.5%Pt/TiO₂(Ca) showed that the latter exhibited superior performance and operated under nearly isothermal conditions with the minimal production of undesired methane. The CO conversion curve could be shifted toward lower temperatures by decreasing the space velocity, demonstrating the feasibility of the metallic monolithic catalyst for small-scale and mobile applications and its potential use in a single-step, medium temperature shift reactor operating in the 300–350 °C range.

Supplementary Materials: The following supporting information can be downloaded at: <https://www.mdpi.com/article/10.3390/catal13020372/s1>, Figure S1: (a) SEM image of the as prepared Pt/TiO₂ catalyst, and EDS mapping results showing the distribution of (b) Pt, (c) O and (d) Ti elements; Figure S2: (a) SEM image of the as prepared TiO₂(Ca) support, and EDS mapping results showing the distribution of (b) Ca, (c) O and (d) Ti elements; Figure S3: (a) SEM image of the Pt/TiO₂(Ca) catalyst and (b) EDS mapping results showing the distribution of Pt element; Figure S4: Effects of the metal content on the performance of bimetallic (0.5%Pt-*x*%M)/TiO₂ catalysts (*x* = 0.5 or 5.0; M = Fe or Cr) under (A) HTS and (B) LTS conditions. Experimental conditions same as in Figure 3; Figure S5: Effects of total flow rate on the performance of Pt/TiO₂(Ca) catalysts coated on the channels of the ceramic monolith: (A) Conversion of CO and (B) yield of CH₄ under HTS conditions. (C) Conversion of CO under LTS conditions. Other experimental conditions same as in Figure 5; Figure S6: Temperature profile along the Pt/TiO₂(Ca)-coated metallic monolith (inlet at *L* = 0) at the indicated total flow rates under the (a) HTS and (b) LTS reaction conditions shown in Figure 6; Figure S7: Temperature profile along the Pt/TiO₂(Ca)-coated ceramic monolith (inlet at *L* = 0) at the indicated total flow rates under the (a) HTS and (b) LTS reaction conditions shown in Figure 6.

Author Contributions: Conceptualization, A.K., G.B., P.P. and D.I.K.; Methodology, A.K., G.B. and D.I.K.; Software, A.K. and G.B.; Validation, A.K., G.B., P.P. and D.I.K.; Investigation, A.K. and G.B.; Writing—original draft preparation, A.K., G.B., P.P. and D.I.K.; Writing—review and editing, G.B. and D.I.K.; Supervision, D.I.K. All authors have read and agreed to the published version of the manuscript.

Funding: This research was funded by the European Union and Greek national funds through the Operational Program Competitiveness, Entrepreneurship and Innovation, under the call RESEARCH-CREATE-INNOVATE (Project acronym: “Eco-Bio-H₂-FCs”, project code: MIS 5074538/T2EAK 00955).

Data Availability Statement: Not applicable.

Conflicts of Interest: The authors declare no conflict of interest.

References

1. Ratnasamy, C.; Wagner, J.P. Water Gas Shift Catalysis. *Catal. Rev.* **2009**, *51*, 325–440. [[CrossRef](#)]
2. Smith, R.J.B.; Loganathan, M.; Shantha, M.S. A Review of the Water Gas Shift Reaction Kinetics. *Int. J. Chem. React. Eng.* **2010**, *8*, Review R4. [[CrossRef](#)]
3. Pal, D.; Chand, R.; Upadhyay, S.; Mishra, P. Performance of water gas shift reaction catalysts: A review. *Renew. Sustain. Energy Rev.* **2018**, *93*, 549–565. [[CrossRef](#)]
4. Chen, W.-H.; Chen, C.-Y. Water gas shift reaction for hydrogen production and carbon dioxide capture: A review. *Appl. Energy* **2020**, *258*, 114078. [[CrossRef](#)]
5. Baraj, E.; Ciahotný, K.; Hlinčík, T. The water gas shift reaction: Catalysts and reaction mechanism. *Fuel* **2021**, *288*, 119817. [[CrossRef](#)]
6. Farrauto, R.J.; Liu, Y.; Ruettinger, W.; Ilinich, O.; Shore, L.; Giroux, T. Precious Metal Catalysts Supported on Ceramic and Metal Monolithic Structures for the Hydrogen Economy. *Catal. Rev.* **2007**, *49*, 141–196. [[CrossRef](#)]
7. Panagiotopoulou, P. Effect of morphological characteristics of TiO₂-supported noble metal catalysts on their activity for the water-gas shift reaction. *J. Catal.* **2004**, *225*, 327–336. [[CrossRef](#)]
8. Panagiotopoulou, P.; Kondarides, D.I. Effect of the nature of the support on the catalytic performance of noble metal catalysts for the water-gas shift reaction. *Catal. Today* **2006**, *112*, 49–52. [[CrossRef](#)]
9. Ebrahimi, P.; Kumar, A.; Khraisheh, M. A review of recent advances in water-gas shift catalysis for hydrogen production. *Emergent Mater.* **2020**, *3*, 881–917. [[CrossRef](#)]
10. Giroux, T.; Hwang, S.; Liu, Y.; Ruettinger, W.; Shore, L. Monolithic structures as alternatives to particulate catalysts for the reforming of hydrocarbons for hydrogen generation. *Appl. Catal. B Environ.* **2005**, *56*, 95–110. [[CrossRef](#)]

11. Du, X.; Gao, D.; Yuan, Z.; Liu, N.; Zhang, C.; Wang, S. Monolithic Pt/Ce_{0.8}Zr_{0.2}O₂/cordierite catalysts for low temperature water gas shift reaction in the real reformat. *Int. J. Hydrogen Energy* **2008**, *33*, 3710–3718. [[CrossRef](#)]
12. Marín, P.; Ordóñez, S.; Díez, F.V. Performance of reverse flow monolithic reactor for water–gas shift reaction. *Catal. Today* **2009**, *147*, S185–S190. [[CrossRef](#)]
13. Özyönüm, G.N.; Yildirim, R. Water gas shift activity of Au–Re catalyst over microstructured cordierite monolith wash-coated by ceria. *Int. J. Hydrogen Energy* **2016**, *41*, 5513–5521. [[CrossRef](#)]
14. González-Castaño, M.; Ivanova, S.; Laguna, O.H.; Martínez, T.L.M.; Centeno, M.; Odriozola, J. Structuring Pt/CeO₂/Al₂O₃ WGS catalyst: Introduction of buffer layer. *Appl. Catal. B Environ.* **2017**, *200*, 420–427. [[CrossRef](#)]
15. García-Moncada, N.; Groppi, G.; Beretta, A.; Romero-Sarria, F.; Odriozola, J.A. Metal Micro-Monoliths for the Kinetic Study and the Intensification of the Water Gas Shift Reaction. *Catalysts* **2018**, *8*, 594. [[CrossRef](#)]
16. Palma, V.; Ruocco, C.; Cortese, M.; Martino, M. Recent Advances in Structured Catalysts Preparation and Use in Water-Gas Shift Reaction. *Catalysts* **2019**, *9*, 991. [[CrossRef](#)]
17. Portela, R.; Wolf, P.; Marinkovic, J.M.; Serrano-Lotina, A.; Riisager, A.; Haumann, M. Tailored monolith supports for improved ultra-low temperature water-gas shift reaction. *React. Chem. Eng.* **2021**, *6*, 2114–2124. [[CrossRef](#)]
18. Panagiotopoulou, P.; Kondarides, D.I. Effects of alkali promotion of TiO₂ on the chemisorptive properties and water–gas shift activity of supported noble metal catalysts. *J. Catal.* **2009**, *267*, 57–66. [[CrossRef](#)]
19. Panagiotopoulou, P.; Kondarides, D.I. Effects of promotion of TiO₂ with alkaline earth metals on the chemisorptive properties and water–gas shift activity of supported platinum catalysts. *Appl. Catal. B Environ.* **2011**, *101*, 738–746. [[CrossRef](#)]
20. Panagiotopoulou, P.; Kondarides, D.I. Effects of alkali additives on the physicochemical characteristics and chemisorptive properties of Pt/TiO₂ catalysts. *J. Catal.* **2008**, *260*, 141–149. [[CrossRef](#)]
21. I Halkides, T.; I Kondarides, D.; E Verykios, X. Catalytic reduction of NO by C₃H₆ over Rh/TiO₂ catalysts: Effect of W₆₊-cation doping of TiO₂ on morphological characteristics and catalytic performance. *Appl. Catal. B Environ.* **2003**, *41*, 415–426. [[CrossRef](#)]
22. Alexeev, O.S.; Chin, S.Y.; Engelhard, M.H.; Ortiz-Soto, L.; Amiridis, M.D. Effects of Reduction Temperature and Metal–Support Interactions on the Catalytic Activity of Pt/γ-Al₂O₃ and Pt/TiO₂ for the Oxidation of CO in the Presence and Absence of H₂. *J. Phys. Chem. B* **2005**, *109*, 23430–23443. [[CrossRef](#)] [[PubMed](#)]
23. Tauster, S.J.; Fung, S.C.; Garten, R.L. Strong metal-support interactions. Group 8 noble metals supported on titanium dioxide. *J. Am. Chem. Soc.* **1978**, *100*, 170–175. [[CrossRef](#)]
24. Haller, G.L.; Resasco, D.E. Metal–Support Interaction: Group VIII Metals and Reducible Oxides. *Adv. Catal.* **1989**, *36*, 173–235. [[CrossRef](#)]
25. Huang, R.; Kwon, O.; Lin, C.; Gorte, R.J. The effects of SMSI on m-Cresol hydrodeoxygenation over Pt/Nb₂O₅ and Pt/TiO₂. *J. Catal.* **2021**, *398*, 102–108. [[CrossRef](#)]
26. He, K.; Wang, Q. Activation of Pt Nanoclusters on TiO₂ via Tuning the Metallic Sites to Promote Low-Temperature CO Oxidation. *Catalysts* **2021**, *11*, 1280. [[CrossRef](#)]
27. Panagiotopoulou, P.; Kondarides, D.; Verykios, X.E. Selective methanation of CO over supported noble metal catalysts: Effects of the nature of the metallic phase on catalytic performance. *Appl. Catal. A Gen.* **2008**, *344*, 45–54. [[CrossRef](#)]
28. Cybulski, A.; Moulijn, J.A. Modelling of heat transfer in metallic monoliths consisting of sinusoidal cells. *Chem. Eng. Sci.* **1994**, *49*, 19–27. [[CrossRef](#)]
29. Tronconi, E.; Groppi, G. A study on the thermal behavior of structured plate-type catalysts with metallic supports for gas/solid exothermic reactions. *Chem. Eng. Sci.* **2000**, *55*, 6021–6036. [[CrossRef](#)]
30. Van Dijk, H.; Boon, J.; Nyqvist, R.; Brink, R.V.D. Development of a single stage heat integrated water-gas shift reactor for fuel processing. *Chem. Eng. J.* **2010**, *159*, 182–189. [[CrossRef](#)]
31. Palma, V.; Pisano, D.; Martino, M. Comparative Study Between Aluminum Monolith and Foam as Carriers for The Intensification of The CO Water Gas Shift Process. *Catalysts* **2018**, *8*, 489. [[CrossRef](#)]
32. Wang, H.; Mao, D.; Qi, J.; Zhang, Q.; Ma, X.; Song, S.; Gu, L.; Yu, R.; Wang, D. Hollow Multishelled Structure of Heterogeneous Co₃O₄–CeO_{2–x} Nanocomposite for CO Catalytic Oxidation. *Adv. Funct. Mater.* **2019**, *29*, 1806588. [[CrossRef](#)]
33. Wang, Z.; Qi, J.; Yang, N.; Yu, R.; Wang, D. Core–shell nano/microstructures for heterogeneous tandem catalysis. *Mater. Chem. Front.* **2021**, *5*, 1126–1139. [[CrossRef](#)]

Disclaimer/Publisher’s Note: The statements, opinions and data contained in all publications are solely those of the individual author(s) and contributor(s) and not of MDPI and/or the editor(s). MDPI and/or the editor(s) disclaim responsibility for any injury to people or property resulting from any ideas, methods, instructions or products referred to in the content.